nature geoscience

ARTICLES
https://doi.org/10.1038/s41561-020-0638-6

Check for updates

Persistently well-ventilated intermediate-depth ocean through the last deglaciation

Tianyu Chen[1,2]✉, Laura F. Robinson[2], Andrea Burke[3], Louis Claxton[2], Mathis P. Hain[4], Tao Li[1,2], James W. B. Rae[3], Joseph Stewart[2], Timothy D. J. Knowles[5], Daniel J. Fornari[6] and Karen S. Harpp[7]

During the last deglaciation (~18–11 thousand years ago), existing radiocarbon (^{14}C) reconstructions of intermediate waters in the mid- to low-latitude oceans show widely diverging trends, with some broadly tracking the atmosphere and others suggesting extreme depletions. These discrepancies cloud our understanding of the deglacial carbon cycle because of the diversity of hypotheses needed to explain these diverging records, for example, injections of ^{14}C-dead geological carbon, mixing of extremely isolated waters from the abyssal ocean or changes in sites of deep-water ventilation. Here we present absolutely dated deglacial deep-sea coral ^{14}C records of intermediate waters from the Galápagos Platform—close to the largest reported deglacial ^{14}C depletions—together with data from the low-latitude Atlantic. Our records indicate coherent, well-equilibrated intermediate-water ^{14}C ventilation in both oceans relative to the atmosphere throughout the deglaciation. The observed overall trend towards ^{14}C-enriched signatures in our records is largely due to enhanced air–sea carbon isotope exchange efficiency under increasing atmospheric p_{CO_2}. These results suggest that the ^{14}C-depleted signatures from foraminifera are likely sedimentary rather than water mass features, and provide tight ^{14}C constraints for modelling changes in circulation and carbon cycle during the last deglaciation.

Natural radiocarbon (^{14}C) is produced in the upper atmosphere, enters the surface ocean via air–sea gas exchange and is transported to depth by the ocean's meridional overturning circulation. Since ^{14}C decays away with a 5,730-year half-life, the ocean's ^{14}C concentration deficit relative to the atmosphere can be used as a chronometer of ocean circulation and a metric of air–sea gas exchange efficiency. Today, the most ^{14}C-depleted signature is found in the deep Northeast Pacific with $\Delta^{14}C$ (for modern seawater, $\Delta^{14}C = (Fm \times \exp(-t/8{,}267) - 1) \times 1{,}000$, where Fm is the fraction modern of the sample and t is years elapsed from AD 1950 until the year of the sample measurement) difference from the pre-bomb atmosphere of ~240‰ (ref. [1]). The ^{14}C records suggest that, during the Last Glacial Maximum (LGM, ~22–19 thousand years ago (ka)), large parts of the Pacific and Atlantic were much more ^{14}C depleted than today, indicative of reduced exchange of carbon between the deep ocean and the atmosphere[2]. This carbon isolation in the deep ocean is thought to account for much of the drawdown of atmospheric CO_2 at the LGM compared with the pre-industrial[3] and results from coupled changes in circulation and biological sequestration of carbon in the deep ocean[4]. The widely held view is that deglacial reinvigoration of ocean overturning brought ^{14}C from the surface to the abyss and at the same time released the ^{14}C-depleted 'old' carbon from the deep ocean to the upper ocean and atmosphere.

However, the impact of deglacial overturning circulation on upper-ocean ^{14}C ventilation is highly controversial. The presence of anomalously old ^{14}C excursions at intermediate depths during deglaciation has been used as evidence for reconnection of an extremely isolated deep carbon reservoir with the upper ocean (that is, above the main thermocline) and the atmosphere via Southern Ocean upwelling and Antarctic intermediate waters (AAIW) advection[5]. Other suggested pathways of abyssal carbon release have included ventilation in the North Pacific[6–8] or from the Arctic into the North Atlantic[9]. Alternatively, it has also been proposed that ^{14}C-free carbon from sources such as submarine volcanism or methane clathrates were injected into intermediate depths of the ocean, for example, in the eastern equatorial Pacific (EEP), and may have contributed to the atmospheric CO_2 rise during the last deglaciation[10,11]. Robust reconstructions of ^{14}C at intermediate depths are thus crucial in constraining the nature of deep-ocean carbon release to the atmosphere and potential links to changes in ocean circulation and climate.

Deglacial intermediate-water ^{14}C reconstructions

Currently, the available deglacial ^{14}C records from the intermediate-depth ocean show a much larger range of variability than deep-ocean or atmospheric records. While some records from benthic foraminifera show anomalies of more than 8,000 years from the atmosphere[10], others do not contain any discernible episodes of large ^{14}C depletion[12–14]. Reliable interpretation of ^{14}C ventilation history for sediment-based records (mainly benthic foraminifera) is critically dependent on age-model assumptions. As an example, the same set of benthic ^{14}C data could indicate either a constant modern-like ^{14}C ventilation of deglacial AAIW[12] or a significant decrease in benthic $\Delta^{14}C$ by more than 150‰ during Heinrich Stadial 1 (HS1) depending on the choice of age model[15]. Notably,

[1]State Key Laboratory for Mineral Deposits Research, School of Earth Sciences and Engineering, Nanjing University, Nanjing, China. [2]School of Earth Sciences, University of Bristol, Bristol, UK. [3]School of Earth and Environmental Sciences, University of St Andrews, St Andrews, UK. [4]Earth and Planetary Sciences, University of California Santa Cruz, Santa Cruz, CA, USA. [5]School of Chemistry, University of Bristol, Bristol, UK. [6]Department of Geology and Geophysics, Woods Hole Oceanographic Institution, Woods Hole, MA, USA. [7]Geology Department, Colgate University, Hamilton, NY, USA.
✉e-mail: tianyuchen@nju.edu.cn

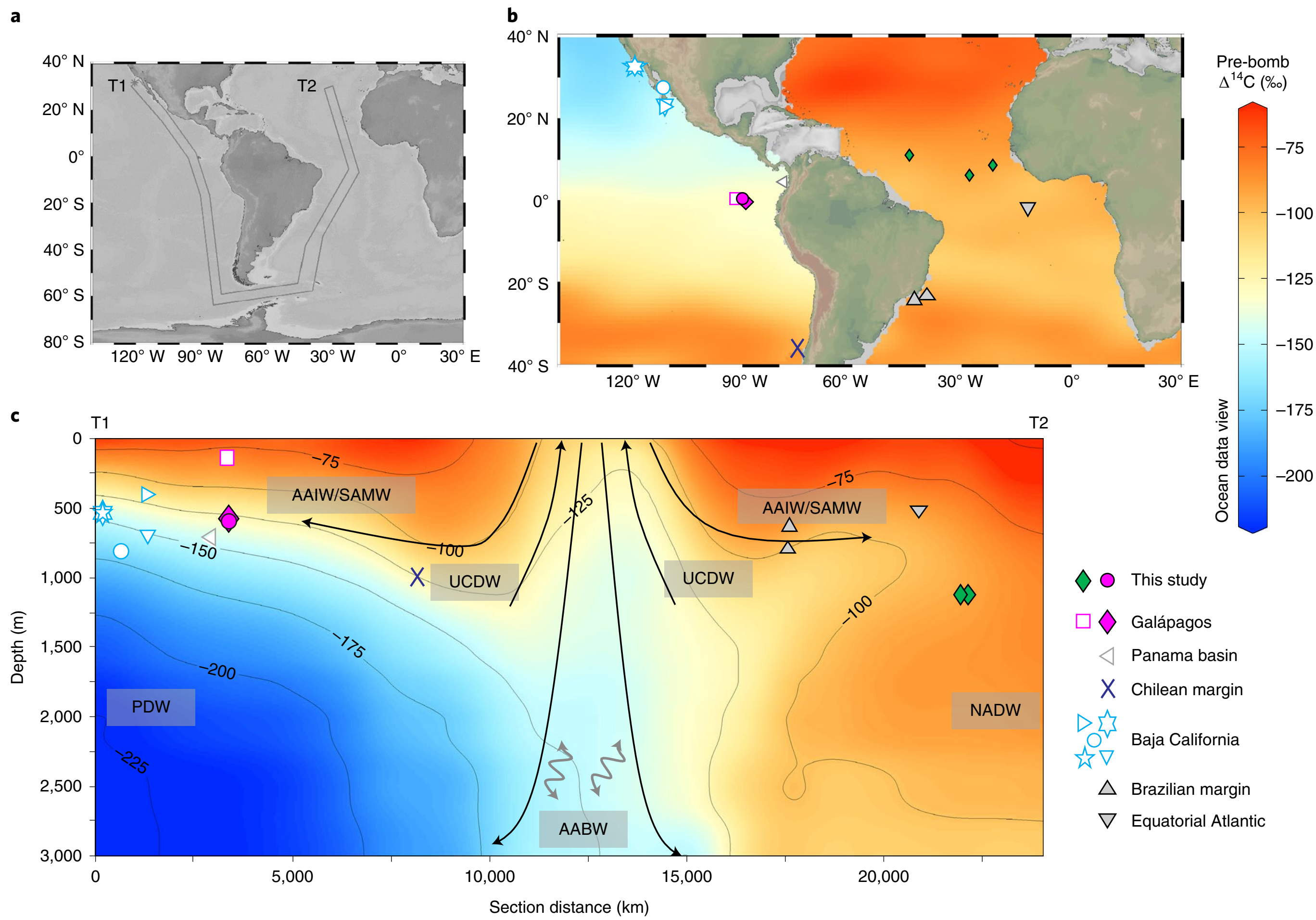

Fig. 1 | Map of sample locations and estimated distribution of pre-bomb ^{14}C concentration. a, Map showing the selected Pacific–Atlantic transection. **b**, Estimated pre-bomb ^{14}C activity of the modern time at water depth of ~700 m (ref. [1]). **c**, Estimated pre-bomb ^{14}C activity of the Pacific–Atlantic transection[1]. Symbols are sites of this study and existing ^{14}C reconstructions in the mid-low latitudes. Solid arrows indicate circulation of the major global water masses[33]. PDW, Pacific Deep Water; SAMW, Subantarctic Mode Water; UCDW, Upper Circumpolar Deep Water; AABW, Antarctic Bottom Water.

the reported ^{14}C data discrepancies are particularly pronounced in the intermediate waters of the EEP (Figs. 1 and 2 and Extended Data Fig. 1), yielding different numbers of occurrences, magnitudes and durations of ^{14}C-depletion episodes over the last deglaciation. While more-recent detrital wood-based chronologies avoid the difficulties of variable surface reservoir ages or uncertainties in age correlation to ice-core/speleothem records, wood-based studies from the EEP also show different magnitudes of ^{14}C depletions[14,16]. These results make it challenging to obtain a consistent picture of upper-ocean ventilation and carbon-cycle changes.

As an archive of past seawater chemistry, deep-sea corals can alleviate some of the complications from sedimentary processes, such as bioturbation and diagenesis within restricted pore-water environments, because they live above the sediment–water interface. In addition, uranium series ages, which can be determined from their aragonite skeletons, are not influenced by ^{14}C surface reservoir ages or tie-point correlation uncertainties. We present uranium series dated ^{14}C records from two sites at ~600 m in the EEP and ~1,100 m in the low-latitude Atlantic. The deep-sea coral-based EEP record largely follows the trajectory of the atmosphere during the deglaciation at the resolution of the data (Fig. 2), and the low-latitude Atlantic sample set follows a similar pattern (Extended Data Fig. 1b). Specifically, the coral-based Δ^{14}C reconstruction of the EEP shows that Δ^{14}C decreased from 170‰ in the early part of the HS1 to 20‰ in the early Holocene. The proportional offset of Δ^{14}C relative to the contemporaneous atmosphere ($\Delta\Delta^{14}C_{corr}$, equivalent to previously reported $\Delta^{14}C_{0,adj}$[17], Extended Data Fig. 1 and Methods) reveals that our data show no major ^{14}C excursions compared with other published records, some of which show large and variable ^{14}C offsets. When converted to a ^{14}C 'age', the sample ^{14}C age offset from the contemporary atmosphere (B-Atm) of EEP intermediate waters decreased from ~1,300 ^{14}C years in the early part of HS1 to ~850 ^{14}C years in the Holocene (Fig. 3e). Much of this change follows the trend expected due to the deglacial increase in atmospheric p_{CO_2} (Fig. 3a and Methods), which increases the rate of carbon isotope exchange between the atmosphere and the surface ocean[18]. Data from equatorial Atlantic intermediate waters exhibit a broadly similar trend to the EEP but are consistently better ventilated throughout the last deglaciation by approximately 20–30‰. This difference is small and mostly within the uncertainties of the data (Extended Data Fig. 1b).

Our EEP data are in marked contrast with an existing foraminifera-based sediment record also from the Galápagos platform, at virtually the same depth (617 m) as our coral-based data (Figs. 1 and 2). The foraminifera-based record shows $\Delta\Delta^{14}C_{corr}$ as low as −670‰ (ref. [10]) (Extended Data Fig. 1d). Given that this excursion is too large to be explained by any recorded deep-water signal, upwelling of carbon from abyssal waters was ruled out, and the release of ^{14}C-free carbon from clathrates or nearby volcanic provinces was put forward as a possible mechanism[10]. Due to the

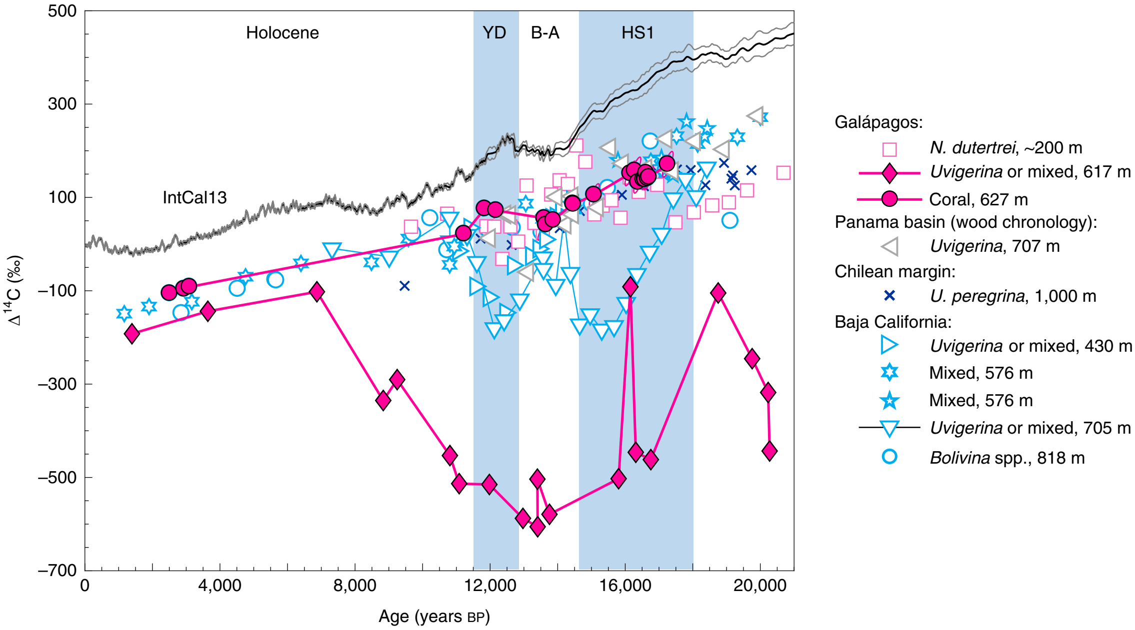

Fig. 2 | The Δ^{14}C records of the eastern Pacific over the past 20 kyr (refs. [5,10,12–14,34–38]). IntCal13 shows the atmosphere Δ^{14}C evolution with ±2σ uncertainty[39]. Symbols are the same as in Fig. 1. The 2σ error ellipses of published data and detailed data comparison can be found in Extended Data Fig. 1. YD, Younger Drayes; B-A, Bølling-Allerød.

proximity and similar water depths, our data provide strong evidence that the hypothesized geological carbon release did not control the ^{14}C content of intermediate waters near Galápagos. More widely, other foraminifera-based records from the low-latitude eastern Pacific near Baja California show variable degrees of ^{14}C depletion during the deglaciation, though never reaching values as low as the foraminifera from Galápagos. It hence seems plausible to invoke geologic or aged sedimentary-carbon release into pore waters to explain the foraminiferal ^{14}C anomalies at both Galápagos and Baja California. By contrast, some Baja California benthic ^{14}C records (Extended Data Fig. 1c) are aligned with our deglacial deep-sea coral ^{14}C evolution, further arguing against regionally substantial deglacial water mass ^{14}C depletions and in favour of localized offsets in pore waters (Methods). Taking a global view, the absence of any discernible episodes of severe ^{14}C depletion in our precisely dated intermediate-water records suggests that basin-scale ^{14}C depletion of upper-ocean water masses is unlikely to have been prevalent. The relatively well-equilibrated intermediate ^{14}C signatures are in agreement with model predictions[19] and imply short residence time for carbon in the upper ocean due to global air–sea gas exchange similar to the present[19,20].

Well-equilibrated intermediate-water ^{14}C ventilation

Today, the ^{14}C signature of the equatorial Atlantic at ~1,100 m is similar to the EEP at around ~600 m (Fig. 1). Both sites are fed partly by AAIW; however, a fraction of ^{14}C-enriched North Atlantic Deep Water (NADW) entrains into the equatorial Atlantic intermediate depths, while ^{14}C-depleted North Pacific water contributes a higher proportion to EEP intermediate depths. Modelling and proxy records from the subarctic North Pacific indicate that unlike the modern day, North Pacific convection may have reached below ~2 km in the early deglaciation[6] between 17 and 16 ka, when the Atlantic meridional overturning circulation was close to a collapsed state[7,21] (Fig. 3b). Our data from the EEP does not exclude the possibility of short-lived deep convection and deep-water formation in the North Pacific[7] that brings ^{14}C-enriched waters to the abyssal ocean and subsequently to the intermediate EEP. For example, the intermediate-water ^{14}C contents of EEP were enriched and were similar to the equatorial Atlantic at ~16.5 ka (Fig. 3e and Extended Data Fig. 2). Nevertheless, the generally better ^{14}C ventilated signature in the Atlantic records is observed through most of the deglaciation where we have coral-based data.

The coherent signals in the low-latitude coral records from both oceans suggest that our data are representative of the mean ^{14}C evolution of upper-ocean waters, after their long-distance advection and mixing from their high-latitude sources[19]. Theory and modelling[18,19] suggest that the deglacial p_{CO_2} increase would have resulted in a greater overall air–sea CO_2 exchange and more complete ^{14}C/C equilibration, with an inverse scaling between surface-water ^{14}C-reservoir ages and p_{CO_2}. The offsets of our data from this simple scaling (baseline in Fig. 3e, Extended Data Fig. 2) are small, suggesting this equilibration mechanism could explain most of the overall deglacial decline in intermediate-water B-Atm age without invoking circulation change. In addition to changes in air–sea disequilibrium in the surface ocean, these small B-Atm ^{14}C age excursions can be interpreted as the signature of changes in the overturning of the deep ocean and its influence on the intermediate waters, with the impact of changing atmospheric Δ^{14}C propagated into the interior ocean being an additional complicating factor (Methods). For example, the decrease of atmospheric Δ^{14}C during HS1 (Fig. 2) would have left the deep-water reservoirs relatively more ^{14}C enriched at the time of their formation (all else being equal) and thus should result in lower B-Atm ages. On the contrary, our record shows a higher B-Atm age than expected from the p_{CO_2} corrected baseline for the well-resolved equatorial Atlantic (Fig. 3e and Extended Data Fig. 2) from the early (~18 ka) to late (~15–16 ka) HS1, thus pointing towards increased connection of the intermediate waters with isolated deep waters, following reduced NADW formation[21] with increased North Atlantic surface reservoir ages[22,23], enhanced upwelling of circumpolar deep waters[24] associated with intensified Southern Ocean convection and Southern Hemisphere westerlies[25], and/or progressively deeper upwelling and ventilation[26]. Subsequently, at the HS1 to Bølling–Allerød transition (that is, 15–14.6 ka), atmospheric Δ^{14}C declined more rapidly than the intermediate water records, yielding

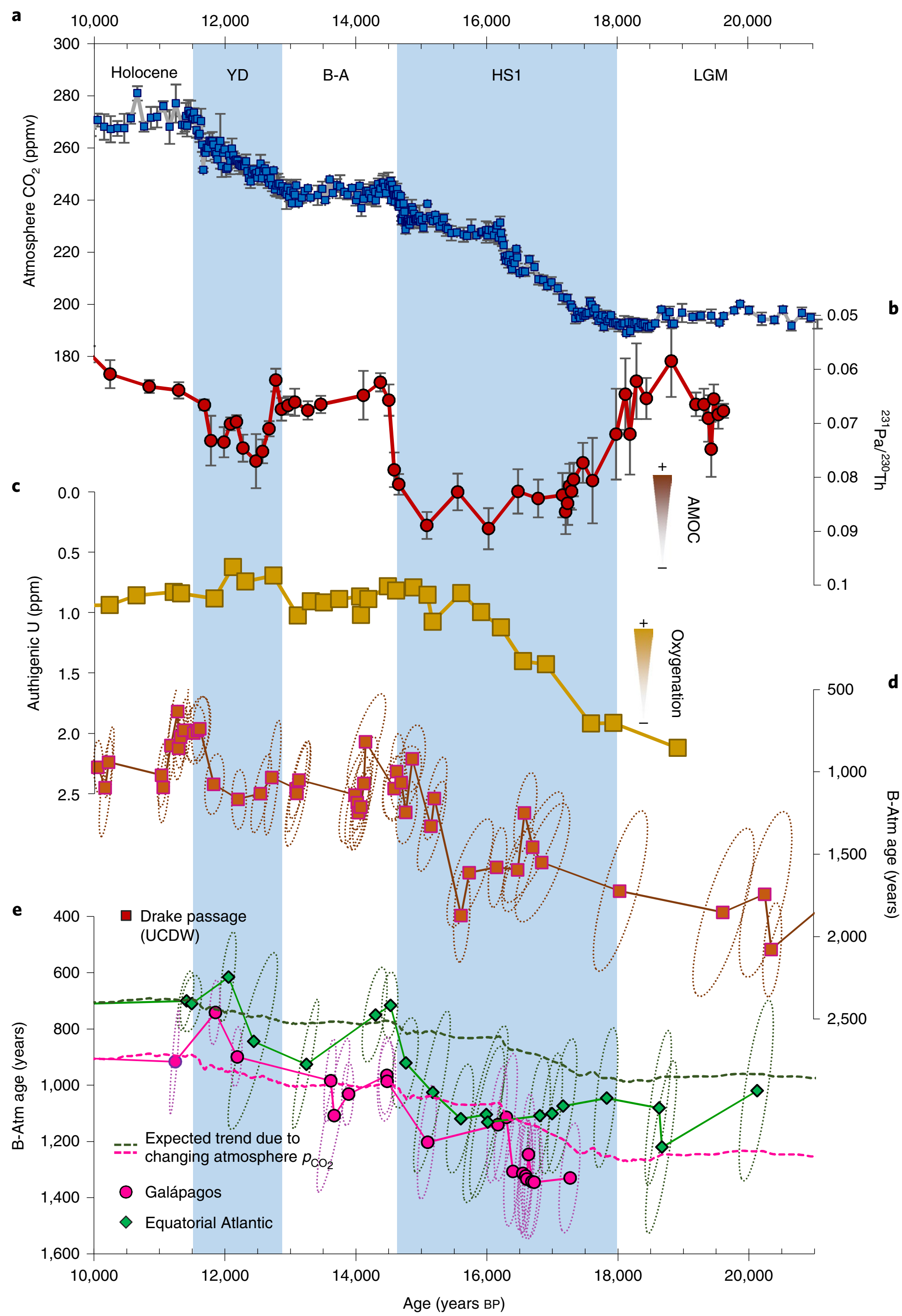

Fig. 3 | The evolution of B-Atm age of our coral records together with other palaeoclimate reconstructions. a, Atmosphere CO_2 concentration[40]. **b**, $^{231}Pa/^{230}Th$ ratios of sediment core OCE326-GGC5 from the deep subtropical North Atlantic[21]. **c**, Sedimentary authigenic U concentrations as a deep-water oxygenation proxy from a deep Southern Ocean sediment core (TN057-13PC)[31]. **d**, B-Atm age evolution of UCDW recorded by deep-sea corals of Drake Passage[13,41]. **e**, B-Atm age evolution of low-latitude intermediate waters (this study). Dashed green and pink lines represent the scenario with atmosphere p_{CO_2} as the only factor affecting ^{14}C-reservoir age for the EEP and equatorial Atlantic intermediate waters, respectively (Methods). Ellipses and bars show the 2σ uncertainties of the data points. Uncertainties are not shown for cases in which they are smaller than the symbols. AMOC, Atlantic meriodonal overturning circulation.

a trend towards better-ventilated oceanic signatures at low latitudes (Fig. 2a) and possibly recording the influence of enhanced formation of ^{14}C-rich NADW at this time[13,27]. Dedicated ocean modelling work (such as applying the transit-time distribution technique[28]) will be needed to precisely deconvolve the ^{14}C effects of physical circulation change, variable surface ocean disequilibrium and variable atmosphere ^{14}C propagated into the interior ocean. Our finding that the observed intermediate-water $\Delta^{14}C$ in the Atlantic and Pacific largely track atmospheric $\Delta^{14}C$ with a predictable p_{CO_2}-dependent offset will be crucially important in these efforts.

Implications for deglacial carbon cycling

Our study provides unique constraints on oceanic carbon-cycle dynamics during the last deglaciation. First, we argue that episodes of anomalous intermediate-depth ^{14}C depletion recorded by benthic foraminifera (Fig. 2 and Extended Data Fig. 1) are very likely to be sedimentary rather than global or basin-scale water mass features. The impact of geological carbon on deglacial carbon cycle must therefore be re-evaluated in climate models in light of the new data obtained in this study. Second, due to the precise age control on deep-sea corals, we can resolve a minor excursion in the well-equilibrated intermediate-water ^{14}C records during HS1 (that is, from ~18 ka to 15–16 ka). This signature is indicative of enhanced mixing of relatively ^{14}C-depleted, presumably carbon-enriched, deep reservoirs with the upper ocean during the early deglaciation, consistent with CO_2 outgassing of low-latitude upwelling zones[29,30] and improved ventilation in the deep Southern Ocean[31] (Fig. 3c) and resulting in atmosphere p_{CO_2} rise (Fig. 3a). Finally, surface ^{14}C-reservoir age variability in the mid- to low-latitude surface oceans is a consequential and much-debated source of uncertainty in dating marine sediment cores on the basis of planktonic foraminifera ^{14}C measurements. Given that surface and thermocline waters are linked by high-latitude upwelling and that surface waters have more carbon isotope exchange with the atmosphere than the intermediate waters at any time, the limited apparent ventilation age changes in our coral-based data would require that surface ^{14}C-reservoir age variability in the mid–low latitudes should also be limited during the last deglaciation, unless there were substantial changes in local subsurface upwelling. Such understanding is consistent with recent surface (0–100 m) reservoir age simulations that show local variability of less than 500 years in the mid–low latitudes (for example, 40° S to 40° N) over the past 20 kyr[32]. Overall, our precise reconstruction of intermediate-water ^{14}C changes yields powerful constraints on mixing between the deep and upper ocean as well as the ocean carbon cycle at the end of the last ice age.

Online content

Any methods, additional references, Nature Research reporting summaries, source data, extended data, supplementary information, acknowledgements, peer review information; details of author contributions and competing interests; and statements of data and code availability are available at https://doi.org/10.1038/s41561-020-0638-6.

Received: 22 February 2020; Accepted: 24 August 2020;
Published online: 12 October 2020

References

1. Key, R. M. et al. A global ocean carbon climatology: results from global data analysis project (GLODAP). *Global Biogeochem. Cycles* **18**, GB4031 (2004).
2. Skinner, L. C. et al. Radiocarbon constraints on the glacial ocean circulation and its impact on atmospheric CO_2. *Nat. Commun.* **8**, 16010 (2017).
3. Monnin, E. et al. Atmospheric CO_2 concentrations over the last glacial termination. *Science* **291**, 112–114 (2001).
4. Sigman, D. M., Hain, M. P. & Haug, G. H. The polar ocean and glacial cycles in atmospheric CO_2 concentration. *Nature* **466**, 47–55 (2010).
5. Marchitto, T. M., Lehman, S. J., Ortiz, J. D., Fluckiger, J. & van Geen, A. Marine radiocarbon evidence for the mechanism of deglacial atmospheric CO_2 rise. *Science* **316**, 1456–1459 (2007).
6. Okazaki, Y. et al. Deepwater formation in the North Pacific during the Last Glacial Termination. *Science* **329**, 200–204 (2010).
7. Rae, J. W. B. et al. Deep water formation in the North Pacific and deglacial CO_2 rise. *Paleoceanography* **29**, 645–667 (2014).
8. Gray, W. R. et al. Deglacial upwelling, productivity and CO_2 outgassing in the North Pacific Ocean. *Nat. Geosci.* **11**, 340–344 (2018).
9. Thornalley, D. J. R. et al. A warm and poorly ventilated deep Arctic Mediterranean during the last glacial period. *Science* **349**, 706–710 (2015).
10. Stott, L., Southon, J., Timmermann, A. & Koutavas, A. Radiocarbon age anomaly at intermediate water depth in the Pacific Ocean during the last deglaciation. *Paleoceanogr. Paleoclimatol.* **24**, PA2223 (2009).
11. Stott, L. D., Harazin, K. M. & Krupinski, N. B. Q. Hydrothermal carbon release to the ocean and atmosphere from the eastern equatorial Pacific during the last glacial termination. *Environ. Res. Lett.* **14**, 025007 (2019).
12. De Pol-Holz, R., Keigwin, L., Southon, J., Hebbeln, D. & Mohtadi, M. No signature of abyssal carbon in intermediate waters off Chile during deglaciation. *Nat. Geosci.* **3**, 192–195 (2010).
13. Chen, T. et al. Synchronous centennial abrupt events in the ocean and atmosphere during the last deglaciation. *Science* **349**, 1537–1541 (2015).
14. Zhao, N. & Keigwin, L. D. An atmospheric chronology for the glacial–deglacial eastern equatorial Pacific. *Nat. Commun.* **9**, 3077 (2018).
15. Siani, G. et al. Carbon isotope records reveal precise timing of enhanced Southern Ocean upwelling during the last deglaciation. *Nat. Commun.* **4**, 2758 (2013).
16. Rafter, P. A., Herguera, J. C. & Southon, J. R. Extreme lowering of deglacial seawater radiocarbon recorded by both epifaunal and infaunal benthic foraminifera in a wood-dated sediment core. *Clim. Past* **14**, 1977–1989 (2018).
17. Cook, M. S. & Keigwin, L. D. Radiocarbon profiles of the NW Pacific from the LGM and deglaciation: evaluating ventilation metrics and the effect of uncertain surface reservoir ages. *Paleoceanogr. Paleoclimatol.* **30**, 174–195 (2015).
18. Galbraith, E. D., Kwon, E. Y., Bianchi, D., Hain, M. P. & Sarmiento, J. L. The impact of atmospheric p_{CO_2} on carbon isotope ratios of the atmosphere and ocean. *Global Biogeochem. Cycles* **29**, 307–324 (2015).
19. Hain, M. P., Sigman, D. M. & Haug, G. H. Shortcomings of the isolated abyssal reservoir model for deglacial radiocarbon changes in the mid-depth Indo-Pacific Ocean. *Geophys. Res. Lett.* **38**, L04604 (2011).
20. Graven, H., Gruber, N., Key, R., Khatiwala, S. & Giraud, X. Changing controls on oceanic radiocarbon: new insights on shallow-to-deep ocean exchange and anthropogenic CO_2 update. *J. Geophys. Res. Oceans* **117**, C10005 (2012).
21. McManus, J. F., Francois, R., Gherardi, J. M., Keigwin, L. D. & Brown-Leger, S. Collapse and rapid resumption of Atlantic meridional circulation linked to deglacial climate changes. *Nature* **428**, 834–837 (2004).
22. Stern, J. V. & Lisiecki, L. E. North Atlantic circulation and reservoir age changes over the past 41,000 years. *Geophys. Res. Lett.* **40**, 3693–3697 (2013).
23. Skinner, L. C., Muschitiello, F. & Scrivner, A. E. Marine reservoir age variability over the last deglaciation: implications for marine carbon cycling and prospects for regional radiocarbon calibrations. *Paleoceanogr. Paleoclimatol.* **34**, 1807–1815 (2019).
24. Anderson, R. F. et al. Wind-driven upwelling in the Southern Ocean and the deglacial rise in atmospheric CO_2. *Science* **323**, 1443–1448 (2009).
25. Menviel, L. et al. Southern Hemisphere westerlies as a driver of the early deglacial atmospheric CO_2 rise. *Nat. Commun.* **9**, 2503 (2018).
26. Lund, D. C., Tessin, A. C., Hoffman, J. L. & Schmittner, A. Southwest Atlantic watermass evolution during the last deglaciation. *Paleoceanogr. Paleoclimatol.* **30**, 477–494 (2015).
27. Barker, S., Knorr, G., Vautravers, M. J., Diz, P. & Skinner, L. C. Extreme deepening of the Atlantic overturning circulation during deglaciation. *Nat. Geosci.* **3**, 567–571 (2010).
28. DeVries, T. & Primeau, F. An improved method for estimating water-mass ventilation age from radiocarbon data. *Earth Planet. Sci. Lett.* **295**, 367–378 (2010).
29. Martinez-Boti, M. A. et al. Boron isotope evidence for oceanic carbon dioxide leakage during the last deglaciation. *Nature* **518**, 219–222 (2015).
30. Shao, J. et al. Atmosphere–ocean CO_2 exchange across the last deglaciation from the boron isotope proxy. *Paleoceanogr. Paleoclimatol.* **34**, 1650–1670 (2019).
31. Jaccard, S. L., Galbraith, E. D., Martinez-Garcia, A. & Anderson, R. F. Covariation of deep Southern Ocean oxygenation and atmospheric CO_2 through the last ice age. *Nature* **530**, 207–210 (2016).
32. Butzin, M., Kohler, P. & Lohmann, G. Marine radiocarbon reservoir age simulations for the past 50,000 years. *Geophys. Res. Lett.* **44**, 8473–8480 (2017).
33. Talley, L. D. Closure of the global overturning circulation through the Indian, Pacific, and Southern Oceans: schematics and transports. *Oceanography* **26**, 80–97 (2013).
34. Ingram, B. I. & Kennett, J. P. Radiocarbon chronology and planktonic-benthic foraminiferal ^{14}C age differences in Santa Barbara Basin sediments, Hole 893A. *Proc. Ocean Drill. Prog. Sci. Results* **146**, 19–27 (1995).
35. Keigwin, L. D. Late Pleistocene–Holocene paleoceanography and ventilation of the Gulf of California. *J. Oceanogr.* **58**, 421–432 (2002).
36. Lindsay, C. M., Lehman, S. J., Marchitto, T. M., Carriquiry, J. D. & Ortiz, J. D. New constraints on deglacial marine radiocarbon anomalies from a depth transect near Baja California. *Paleoceanogr. Paleoclimatol.* **31**, 1103–1116 (2016).
37. Umling, N. E. & Thunell, R. C. Synchronous deglacial thermocline and deep-water ventilation in the eastern equatorial Pacific. *Nat. Commun.* **8**, 14203 (2017).

38. Magana, A. L. et al. Resolving the cause of large differences between deglacial benthic foraminifera radiocarbon measurements in Santa Barbara Basin. *Paleoceanogr. Paleoclimatol.* **25**, PA4102 (2010).
39. Reimer, P. J. et al. Intcal13 and Marine13 radiocarbon age calibration curves 0–50,000 years cal BP. *Radiocarbon* **55**, 1869–1887 (2013).
40. Marcott, S. A. et al. Centennial-scale changes in the global carbon cycle during the last deglaciation. *Nature* **514**, 616–619 (2014).
41. Burke, A. & Robinson, L. F. The Southern Ocean's role in carbon exchange during the last deglaciation. *Science* **335**, 557–561 (2012).

Methods

Materials and analytical methods. The deep-sea corals were collected from the Galápagos platform in the EEP by both dredging and remotely operated vehicle (ROV) and in the low-latitude equatorial Atlantic by ROV[13,42,43] (Extended Data Figs. 3, 4 and 5). Under modern circulation, the studied two sites are in part fed by intermediate/mode water originating from the Southern Ocean, with some inputs from the North Atlantic and North Pacific, so they are well suited to testing hypotheses that link the various pathways of upper–deep ocean mixing and mean state of the upper-ocean ventilation. Aragonite deep-sea corals are insensitive to sedimentary processes because they live above the sediment–water interface. Therefore, deep-sea corals can provide a well-constrained ^{14}C activity of bottom water on a precisely dated absolute age scale. In previous deep-sea coral ^{14}C studies of the Southern Ocean[13,41], for example, the generation of ^{14}C temporal evolution is by linking corals growing on different locations and a range of depths, which could potentially incorporate spatial ^{14}C variability in the temporal evolution records. Nevertheless, an obvious strength in this study is that we reconstruct the deglacial ^{14}C ventilation histories using samples essentially growing at the same locations/depths by a single dredge or ROV dive during sample recovery for both oceans. One set of deglacial samples is from the Galápagos Platform recovered from water depth of ~627 m (Fig. 1, Extended Data Figs. 3, 4 and 5 and Extended Data Table 1). In addition, we present new data (Extended Data Tables 1 and 2 and Extended Data Fig. 6) that fill in a critical gap (late HS1) of an existing ^{14}C record of equatorial Atlantic intermediate waters at water depths of ~1,080 m[13]. This composite record is dominated by samples from a single ROV dive at the eastern Atlantic Carter Seamount, with only a few data points from similar water depths at other seamounts[13] without influencing our data interpretation (Extended Data Fig. 4). Therefore, our samples yield two well-resolved, location-bias free, ^{14}C records since the LGM. In both the Pacific and Atlantic, the intermediate waters sampled by our coral-based datasets are part of the upper-ocean circulation system and should therefore provide reliable constraints on the release of ^{14}C-depleted carbon from either the deep ocean or geologic sources, as well as on the dissipation of that carbon through the upper ocean and atmosphere.

The deep-sea coral from the Galápagos platform are mostly large colonial coral fragments with chunky dense structures. No sign of boring holes or alterations were observed after the samples were cut and cleaned. Uranium–thorium (U–Th) ages of the EEP deep-sea corals have been analysed previously[44]. The intermediate-water ^{14}C record of the equatorial Atlantic is partly based on the published data[13] (that is, group B of the coral samples in that study). In our study, we have analysed more samples mainly from the late HS1 on the basis of the age-screening results using the laser ablation multi-collector inductively coupled plasma mass spectrometry (LA-MC-ICPMS) method developed at the University of Bristol[45]. For U–Th dating of the new coral samples of the equatorial Atlantic, we have followed the method that has been described previously in the same lab[13] and will not be reiterated here. One advantage of the U–Th ages of the coral samples published[13] and new ones in this study is that they were processed in the same way, and therefore no systematic error is expected between different sets of samples. The ^{14}C data of this study were analysed by the new accelerator mass spectrometry (AMS) facility recently installed at the University of Bristol, while coral ^{14}C data published by Chen et al.[13] were measured in the AMS lab of the University of California, Irvine (UCI). We have remeasured some coral samples that were previously analysed in UCI. The results (Extended Data Fig. 6 and Extended Data Table 3) show that the ^{14}C ages analysed in Bristol reproduce quite satisfactorily even if coral samples might themselves contain some inhomogeneity. The pretreatment of the coral samples for ^{14}C measurement in Bristol essentially followed the method of UCI. Each coral sample with weight of approximately 15–20 mg was put into a glass tube for acid leach. We have leached the sample to ~10 mg with hot 0.1 N HCl before graphitization. After the samples were dried, they reacted with concentrated phosphoric acid to produce CO_2, which was transferred into the gas line with helium as the carrier gas to an automated graphitization device. After graphitization, the targets were measured by the MICADAS AMS with acceleration potential of 200 kV. The fossil coral with ages much older than 50 ka graphitized by the automated device typically give blank ^{14}C ages of 46–50 ka. All data are reported after blank correction with 2σ error given in Extended Data Table 1.

^{14}C data report. There are three ways to present ^{14}C data in this study. (1) The first is the known-age ^{14}C correction $\Delta^{14}C$, which is expressed as $\Delta^{14}C_{coral} = (Fm \times e^{(calendar\ age/8,267)} - 1) \times 1,000$. (2) To allow direct comparison for the changing atmosphere ^{14}C inventory, deep-water ^{14}C is often reported as the B-Atm age, which equals $R_{coral} - R_{atmosphere}$. R_{coral} is the ^{14}C age of corals and $R_{atmosphere}$ is the ^{14}C age of the contemporaneous atmosphere. Error propagation of the uncertainties follows those described previously[13] with a Monte Carlo technique. (3) Third is offset of deep-water $\Delta^{14}C$ from the contemporary atmosphere, which is expressed simply as $\Delta\Delta^{14}C = \Delta^{14}C_{coral} - \Delta^{14}C_{atmosphere}$. However, $\Delta\Delta^{14}C$ will change with a changing atmosphere ^{14}C pool, without the true ^{14}C ventilation change. One useful way to apply ^{14}C as a geochemical tracer is to calculate inventory-corrected $\Delta\Delta^{14}C_{corr}$ (ref. [17]), which can be expressed as $\Delta\Delta^{14}C_{corr} = (\exp(\lambda_{Libby} \times (R_{atmosphere} - R_{coral})) - 1) \times 1,000$, where λ is the ^{14}C decay constant calculated from the Libby half-life of 5,568 years, and $R_{atmosphere}$ and R_{coral} are the ^{14}C age of contemporaneous atmosphere and coral sample, respectively. Note this metric is functionally the same as what was defined elsewhere in the literature as $\Delta^{14}C_{atm\ normalized}$ (ref. [46]) and ε (ref. [47]). The $\Delta\Delta^{14}C_{corr}$ has not corrected the impact of variable atmospheric $\Delta^{14}C$ propagated into the interior ocean. Atmosphere ^{14}C evolution is taken from the IntCal13 calibration curve[39].

Possible causes of EEP ^{14}C depletions. While there is growing consensus on more ^{14}C-depleted deep oceans during LGM than today[2,41,47–54], large data scatter is observed at different depths during this period[2]. The ^{14}C data of deep thermocline foraminifera species of the equatorial Atlantic[55] closely track our records, while data of buried deep-sea coral from the Brazilian margin show larger scatter[56] (Extended Data Fig. 1d). Deglacial intermediate-water ^{14}C data in the mid- to low-latitude eastern Pacific published over the past three decades[5,12,14,34–38,57] show most pronounced variability compared with the deep-ocean records (see a recent compilation[58]). It is not yet fully clear what has caused the observed large $\Delta^{14}C$ differences between different records apart from age-model uncertainties and bioturbation, especially in the intermediate waters. There is indeed pockmark evidence for deglacial releases of clathrates to the overlying water[59], but there is no evidence to support their distinct role in the deglacial carbon cycle. Compilation of global occurrences of seep carbonate formation over the last two glacial cycles instead implied that enhanced clathrates release occurred during warm high-sea-level stands[60]. Regarding hydrothermal carbon contribution to the EEP region, it is likely that diffusion of old carbon from depth did not inject in large quantities to the overlying water mass but remained in the pore waters and at sediment–seawater interfaces, causing large excursions in the benthic foraminifera records without greatly affecting bottom waters. Indeed, negative deglacial excursions of $\delta^{13}C$ are observed in benthic foraminifera records of the EEP with different durations and magnitudes probably linked to pore-water chemistry[11,61]. However, it is not possible to reconstruct seawater $\delta^{13}C$ (a measure of the ratio of stable isotopes $^{13}C/^{12}C$, defined as $\delta^{13}C = ((^{13}C/^{12}C)_{sample}/(^{13}C/^{12}C)_{standard} - 1) \times 1,000$) based on the stable carbon isotopes of scleractinian corals because they are strongly regulated by biological vital effects[62]. Therefore, our study is unable to provide independent evaluation from the coral stable isotope perspective. Other possibilities such as diagenetic overprint[63] or species effect[38,64] are also worth investigating, but they appear not to be the fundamental causes for benthic foraminifera ^{14}C depletions in the EEP[10,11].

p_{CO_2} effect. The p_{CO_2} effect describes the phenomenon that atmospheric carbon isotopes exchange more slowly with the seawater when the atmosphere CO_2 concentration is lower[18]. This might result in an increase of surface ^{14}C-reservoir age by ~250 years, which is then rapidly propagated into the intermediate waters, during the LGM compared with the modern, even when ocean circulation remains invariant. It is important to take this effect into account for our precisely dated coral samples that aim to track nuanced changes in the ocean-circulation-induced ^{14}C variability of intermediate waters. Rather than introducing new metrics of the ^{14}C to consider the p_{CO_2} effect, we simply construct two curves as shown in Fig. 3e with Holocene B-Atm ages of 700 and 900 years, respectively. We then assume all else being equal, and the p_{CO_2} effect on ^{14}C-reservoir age is calculated as $\text{B-Atm}_t = \text{B-Atm}_{Holocene} \times (p_{CO_2})_{Holocene} / (p_{CO_2})_t$[18], where t is the calendar age. We also have calculated the ^{14}C age offset of each coral record from the two baseline curves, respectively, which is shown in Extended Data Fig. 2.

Effect of variable atmospheric Δ^{14}C propagated into the interior ocean. The impact of changing atmospheric $\Delta^{14}C$ on initial ^{14}C content of deep waters at the time of their formation makes it challenging to deconvolve ocean circulation changes from small B-Atm ^{14}C age excursions. It is interesting to explore whether the small variability in ventilation age of intermediate waters still holds during the last deglaciation when incorporating the influence of variable atmosphere $\Delta^{14}C$ propagated into the interior ocean. The projection age technique attempts to measure the time lag between the entrainment of surface source waters down to greater depths and the time that this $\Delta^{14}C$ is recorded by benthic organisms (for example, corals or foraminifera, see graphic illustration by Cook et al.[17]). The projection age thus has the potential to take into account the impact of variable atmosphere $\Delta^{14}C$ propagated into the interior ocean. We have calculated the projected age (Extended Data Fig. 7) of the intermediate waters to a hypothetical well-equilibrated surface source (that is, Marine13 calibration curve[39]). In reality, changes in the projection age should reflect combined effects of source-water aging and mixing in the deep ocean, as well as variability of the air–sea exchange disequilibrium in the surface ocean. In our study, a higher projection age could mean more isolated, 'older' source waters supplying the intermediate layers, or reduced surface air–sea carbon isotope exchange of the source waters before subducting into the intermediate layers or a combination of these two effects. Overall, the calculated projection age (Extended Data Fig. 7) has a quite small variability and shows decline by only a few hundred years during the last deglaciation, in corroboration with the understanding based on 'B-Atm age' without considering the impact of variable atmospheric $\Delta^{14}C$ propagated into the interior ocean. In addition, the increasing projection age of the well-resolved Atlantic record from the early (~18 ka) to late (~15–16 ka) HS1 will reinforce our argument on increased mixing of isolated deep waters into the intermediate layers during this period as discussed in the main text. It should be noted that 'projection age' uses a simple assumption about initial ^{14}C signatures of source waters and still could not fully account for the complexity of various sources of deep waters with different ages[28] supplying the intermediate waters. Nevertheless, the coherency of the understanding from the evolution of B-Atm age and projection age lends strong support to our interpretation on ocean circulation change during HS1.

Data availability

Sample location information, U-series ages and radiocarbon data that support the findings of this study are available in Extended Data Tables 1–3 and Mendeley Data https://doi.org/10.17632/vxrmfch8h9.1. The atmosphere CO_2 concentration records, radiocarbon data, $^{231}Pa/^{230}Th$ and authigenic uranium flux cited in this study were previously published in refs. [13,21,31,39–41] and are available in the Source Data. The calculated B-Atm age trend without circulation change as well as projection age of the low-latitude coral samples are also available in the Source Data. Detailed information on published foraminifera age and radiocarbon data are available from a recent comprehensive compilation[58] (https://www.ncdc.noaa.gov/paleo/study/21390). Source data are provided with this paper.

References

42. Robinson, L. F. *RRS James Cook Cruise JC094, October 13–November 30 2013, Tenerife-Trinidad. TROPICS, Tracing Oceanic Processes Using Corals and Sediments. Reconstructing Abrupt Changes in Chemistry and circulation of the Equatorial Atlantic Ocean: Implications for Global Climate and Deep-Water Habitats* (ERC, 2014); https://go.nature.com/32YIOmo
43. Mittelstaedt, E., Soule, A. S., Harpp, K. S. & Fornari, D. in *The Galápagos: A Natural Laboratory for the Earth Sciences* (eds Harpp, K. S. et al.) Ch. 14 (AGU, 2014).
44. Chen, T. et al. Ocean mixing and ice-sheet control of seawater $^{234}U/^{238}U$ during the last deglaciation. *Science* **354**, 626–629 (2016).
45. Spooner, P. T., Chen, T., Robinson, L. F. & Coath, C. D. Rapid uranium-series age screening of carbonates by laser ablation mass spectrometry. *Quat. Geochronol.* **31**, 28–39 (2016).
46. Burke, A. et al. The glacial mid-depth radiocarbon bulge and its implications for the overturning circulation. *Paleoceanogr. Paleoclimatol.* **30**, 1021–1039 (2015).
47. Hines, S. K., Southon, J. R. & Adkins, J. F. A high-resolution record of Southern Ocean intermediate water radiocarbon over the past 30,000 years. *Earth Planet. Sci. Lett.* **432**, 46–58 (2015).
48. Freeman, E., Skinner, L. C., Waelbroeck, C. & Hodell, D. Radiocarbon evidence for enhanced respired carbon storage in the Atlantic at the Last Glacial Maximum. *Nat. Commun.* **7**, 11998 (2016).
49. Keigwin, L. D. & Lehman, S. J. Radiocarbon evidence for a possible abyssal front near 3.1 km in the glacial equatorial Pacific Ocean. *Earth Planet. Sci. Lett.* **425**, 93–104 (2015).
50. Robinson, L. F. et al. Radiocarbon variability in the western North Atlantic during the last deglaciation. *Science* **310**, 1469–1473 (2005).
51. Ronge, T. A. et al. Radiocarbon constraints on the extent and evolution of the South Pacific glacial carbon pool. *Nat. Commun.* **7**, 11487 (2016).
52. Sikes, E. L., Cook, M. S. & Guilderson, T. P. Reduced deep ocean ventilation in the Southern Pacific Ocean during the last glaciation persisted into the deglaciation. *Earth Planet. Sci. Lett.* **438**, 130–138 (2016).
53. Skinner, L. C., Fallon, S., Waelbroeck, C., Michel, E. & Barker, S. Ventilation of the deep Southern Ocean and deglacial CO_2 rise. *Science* **328**, 1147–1151 (2010).
54. Sarnthein, M., Schneider, B. & Grootes, P. M. Peak glacial ^{14}C ventilation ages suggest major draw-down of carbon into the abyssal ocean. *Clim. Past* **9**, 2595–2614 (2013).
55. Cléroux, C. & Guilderson, T. Deglacial radiocarbon history of tropical Atlantic thermocline waters: absence of CO_2 reservoir purging signal. *Quat. Sci. Rev.* **30**, 1875–1882 (2011).
56. Mangini, A. et al. Deep sea corals off Brazil verify a poorly ventilated Southern Pacific Ocean during H2, H1 and the younger dryas. *Earth Planet. Sci. Lett.* **293**, 269–276 (2010).
57. Bova, S. C., Herbert, T. D. & Altabet, M. A. Ventilation of northern and southern sources of aged carbon in the eastern equatorial Pacific during the younger dryas rise in atmospheric CO_2. *Paleoceanogr. Paleoclimatol.* **33**, 1151–1168 (2018).
58. Zhao, N., Marchal, O., Keigwin, L., Amrhein, D. & Gebbie, G. A synthesis of deglacial deep-sea radiocarbon records and their (in)consistency with modern ocean ventilation. *Paleoceanogr. Paleoclimatol.* **33**, 128–151 (2018).
59. Stott, L. et al. CO_2 release from pockmarks on the Chatham Rise–Bounty Trough at the glacial termination. *Paleoceanogr. Paleoclimatol.* **34**, 1726–1743 (2019).
60. Chen, F. et al. Gas hydrate dissociation during sea-level highstand inferred from U/Th dating of seep carbonate from the South China Sea. *Geophys. Res. Lett.* **46**, 13928–13938 (2019).
61. Bova, S. C. et al. Links between eastern equatorial Pacific stratification and atmospheric CO_2 rise during the last deglaciation. *Paleoceanogr. Paleoclimatol.* **30**, 1407–1424 (2015).
62. Adkins, J. F., Boyle, E. A., Curry, W. B. & Lutringer, A. Stable isotopes in deep-sea corals and a new mechanism for "vital effects". *Geochim. Cosmochim. Acta* **67**, 1129–1143 (2003).
63. Wycech, J., Kelly, D. C. & Marcott, S. Effects of seafloor diagenesis on planktic foraminiferal radiocarbon ages. *Geology* **44**, 551–554 (2016).
64. Ezat, M. M. et al. Ventilation history of Nordic Seas overflows during the last (de) glacial period revealed by species-specific benthic foraminiferal ^{14}C dates. *Paleoceanogr. Paleoclimatol.* **32**, 172–181 (2017).

Acknowledgements

This study was funded by the European Research Council, the Natural Environment Research Council (NE/S001743/1; NE/N011716/1), the Philip Leverhulme Trust, the Strategic Priority Research Program of Chinese Academy of Sciences (XDB40010200), the National Natural Science Foundation of China (41822603), the US National Science Foundation (OCE-0926637, OCE-10309040 and OCE-0926491), a Marie Curie Reintegration Grant and the NOAA (National Oceanic and Atmospheric Administration) Ocean Exploration Trust. We also thank the JC094 cruise members, shipboard staff and science party on MV1007 (permit #111-2010), the Charles Darwin Research Station, the Charles Darwin Research Foundation, the Galápagos National Park and INOCAR (Instituto Oceanográfico de la Armada de Ecuador) for supporting the coral sampling.

Author contributions

T.C. and L.F.R. designed the study and wrote the paper. L.F.R., D.J.F. and K.S.H. collected the deep-sea coral samples. T.C., L.C., T.L. and T.D.J.K. did the U-series and ^{14}C analysis. All authors contributed to the discussion on data interpretation and improving the manuscript draft.

Competing interests

The authors declare no competing interests.

Additional information

Extended data is available for this paper at https://doi.org/10.1038/s41561-020-0638-6.

Supplementary information is available for this paper at https://doi.org/10.1038/s41561-020-0638-6.

Correspondence and requests for materials should be addressed to T.C.

Peer review information Primary Handling Editor: James Super.

Reprints and permissions information is available at www.nature.com/reprints.

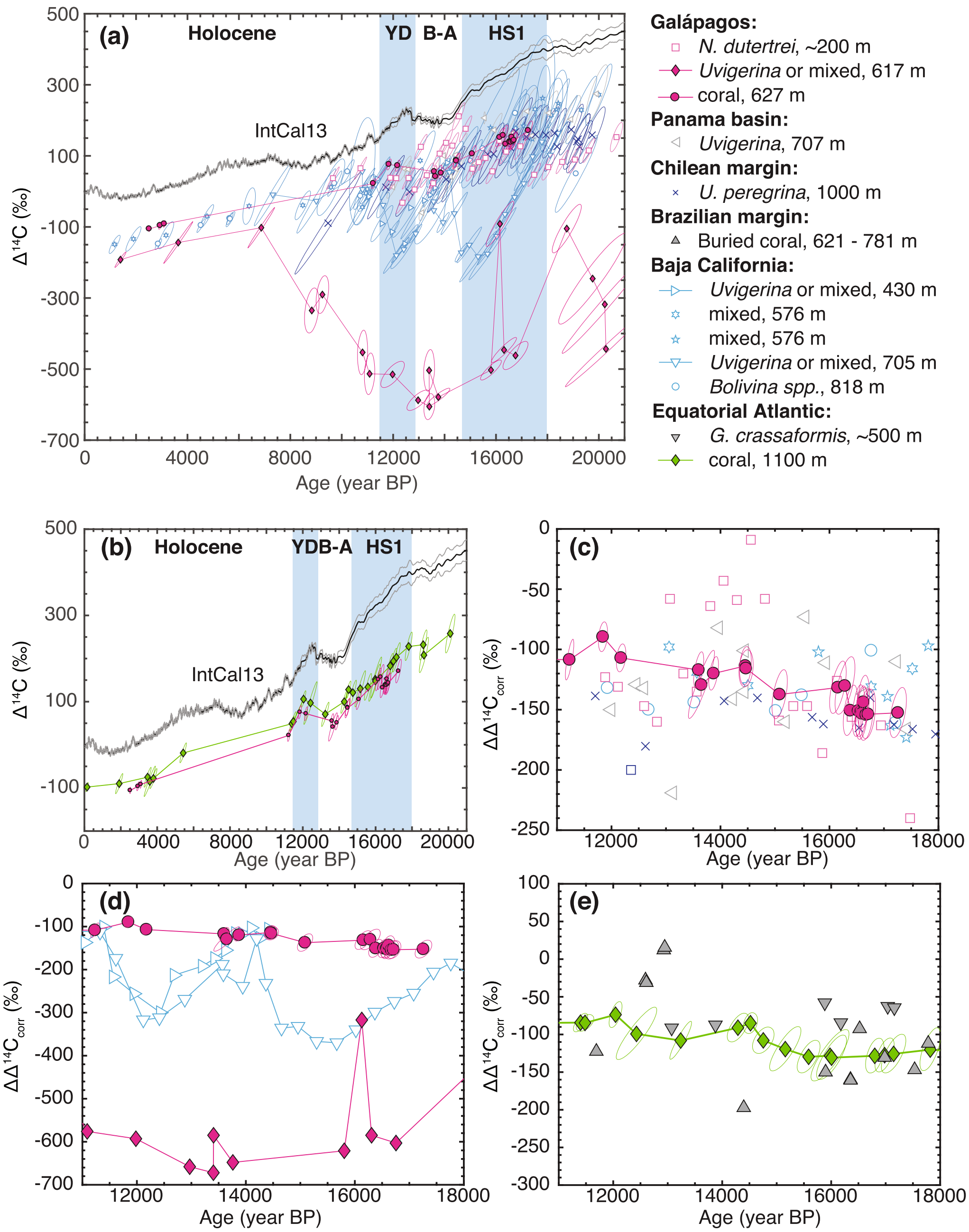

Extended Data Fig. 1 | Compiled ¹⁴C evolution of mid-low latitude intermediate water records during the last deglaciation. (**a**) $\Delta^{14}C$ of the eastern Pacific; (**b**) $\Delta^{14}C$ of the equatorial Pacific and Atlantic corals; (**c**) $\Delta\Delta^{14}C_{corr}$ of eastern Pacific records that did not show large ^{14}C depletions; (**d**) $\Delta\Delta^{14}C_{corr}$ of eastern Pacific records with large ^{14}C depletions in comparison to our data; (**e**) $\Delta\Delta^{14}C_{corr}$ of mid-low latitude Atlantic records. Also shown in (a) is the atmosphere $\Delta^{14}C$ evolution with ±2σ uncertainty[39]. The legend in (a) shows the materials used for the ^{14}C reconstruction[5,10,12–14,34–38,55,56]. Symbols are the same as in Fig. 1. For clarity, 2σ error ellipses of $\Delta\Delta^{14}C_{corr}$ of published data are not shown.

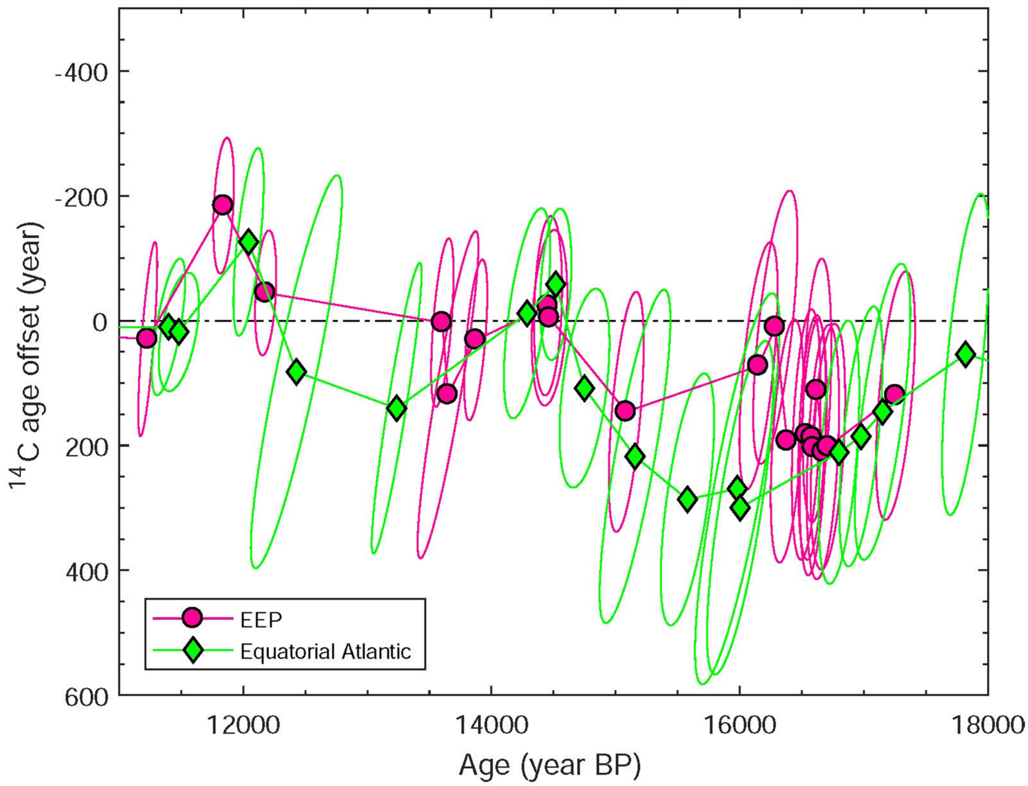

Extended Data Fig. 2 | Radiocarbon age offset of the deep-sea coral data from the expected trend forced by the atmospheric *p*CO_2 induced air-sea isotope exchange efficiency change alone. Note vertical axis is reversed. Zero ^{14}C age offset means a Holocene-like ^{14}C ventilation in the upper ocean.

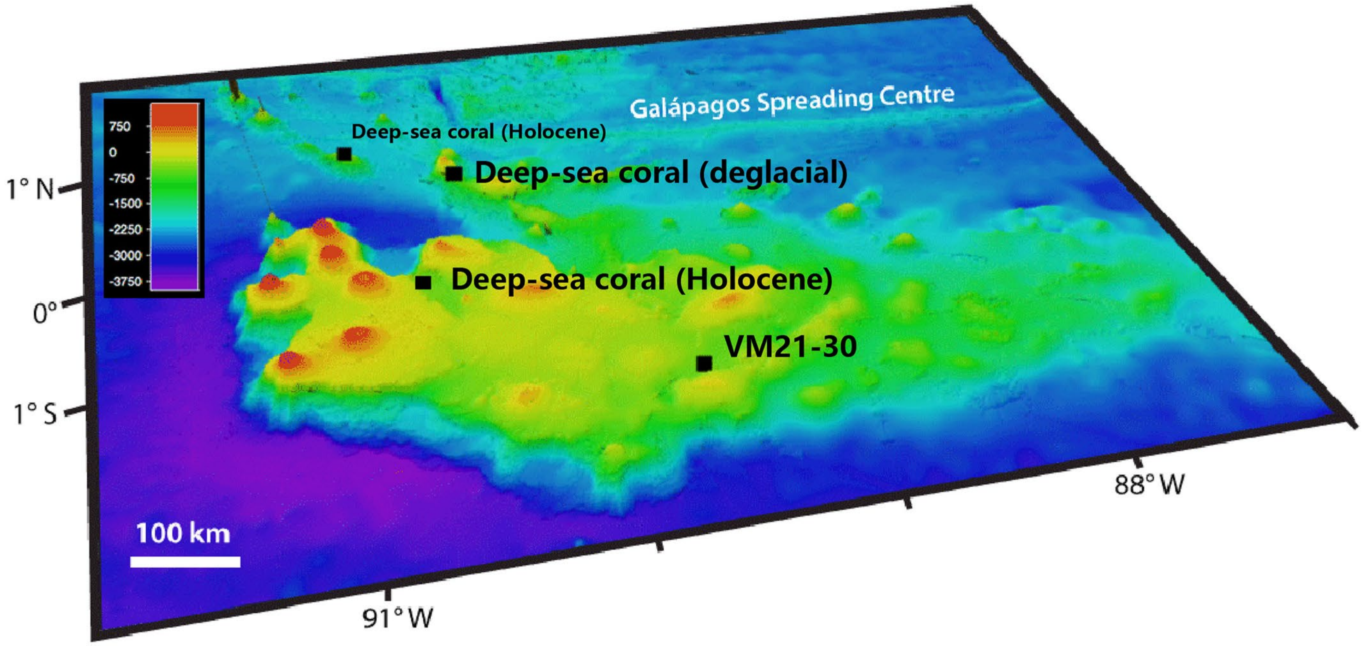

Extended Data Fig. 3 | The bathymetry and sample locations of the Galápagos platform. VM21-30[10] showed the most depleted benthic ^{14}C content during the deglacial period reported so far.

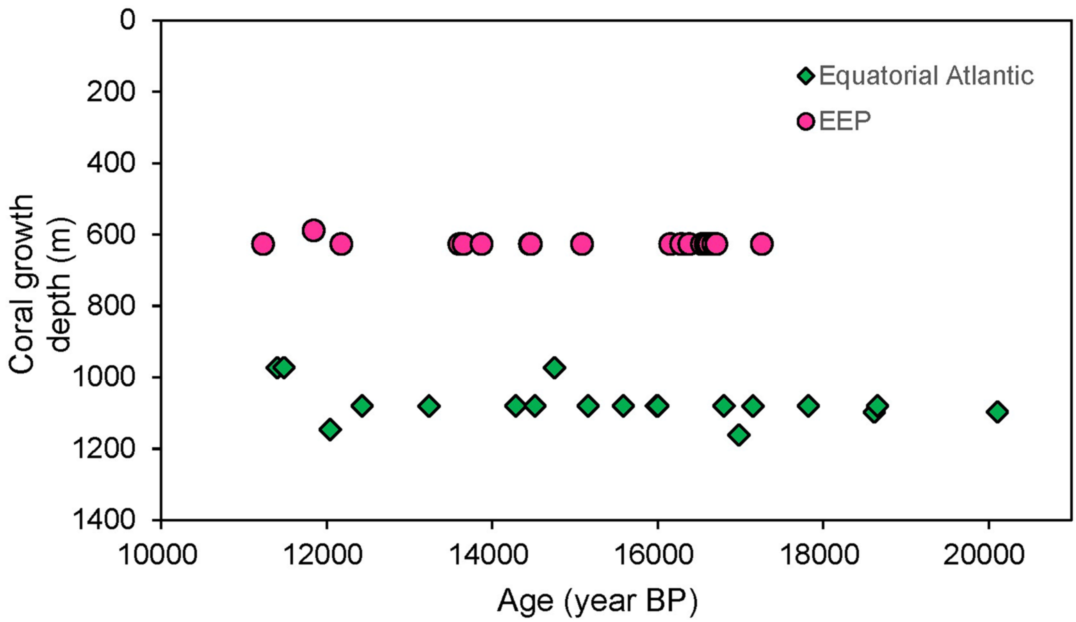

Extended Data Fig. 4 | Age-depth distribution for reported deglacial deep-sea corals. Red dots represent samples from the EEP while the green diamonds represent samples from the Equatorial Atlantic.

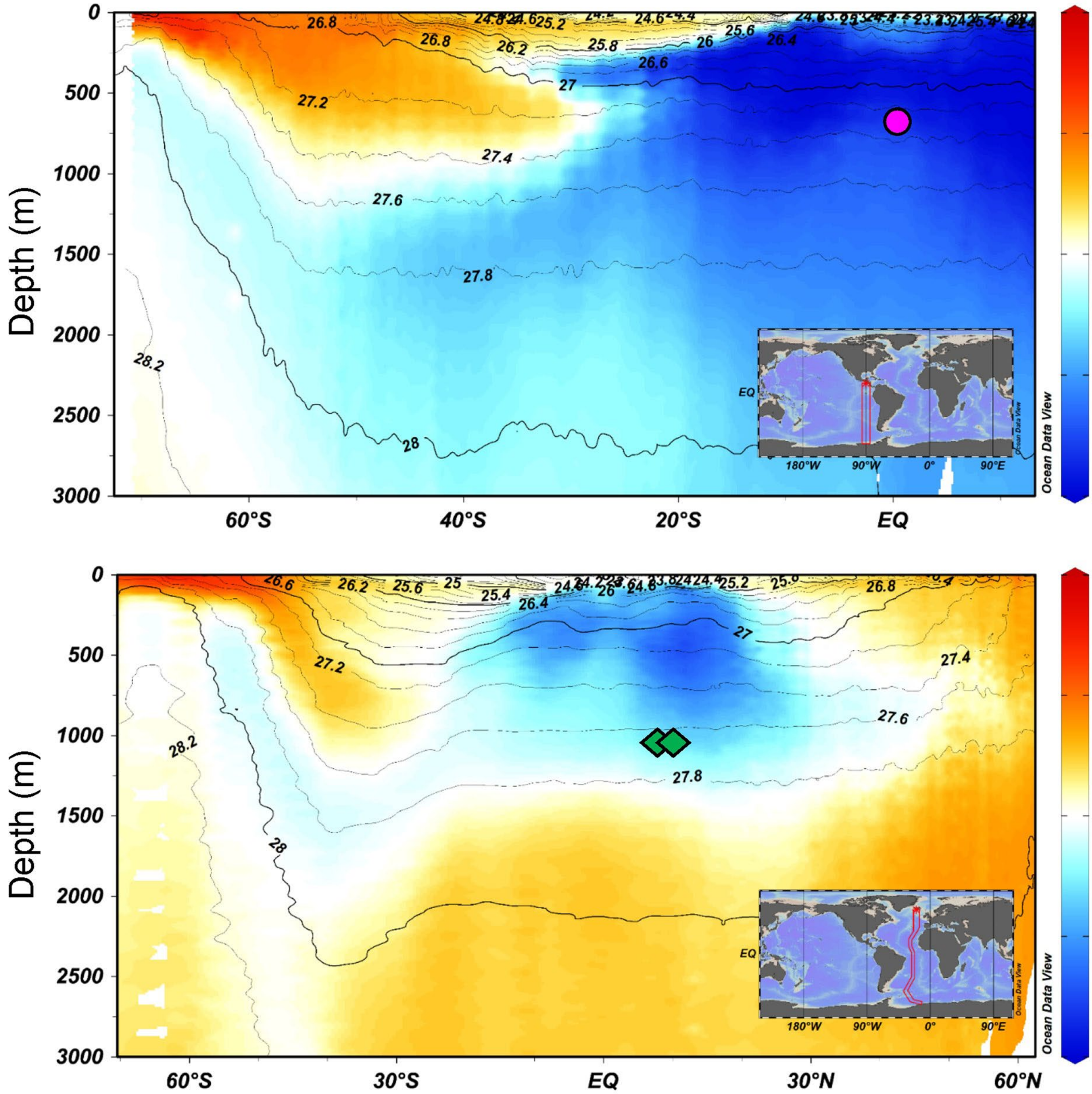

Extended Data Fig. 5 | Sample locations of this study and hydrography of the Pacific and Atlantic transections. Upper panel: Pacific; Lower panel: Atlantic. Colour maps denote oxygen concentrations (μmol/kg) while contours denote neutral densities (kg/m^3). These low-latitude corals located close to or within the oxygen minimum zone as a result of oxygen utilization by remineralization of the falling biogenic particles along the advection path from the high to low latitude oceans. Data were from GLODAP[1] and were plotted with ODV.

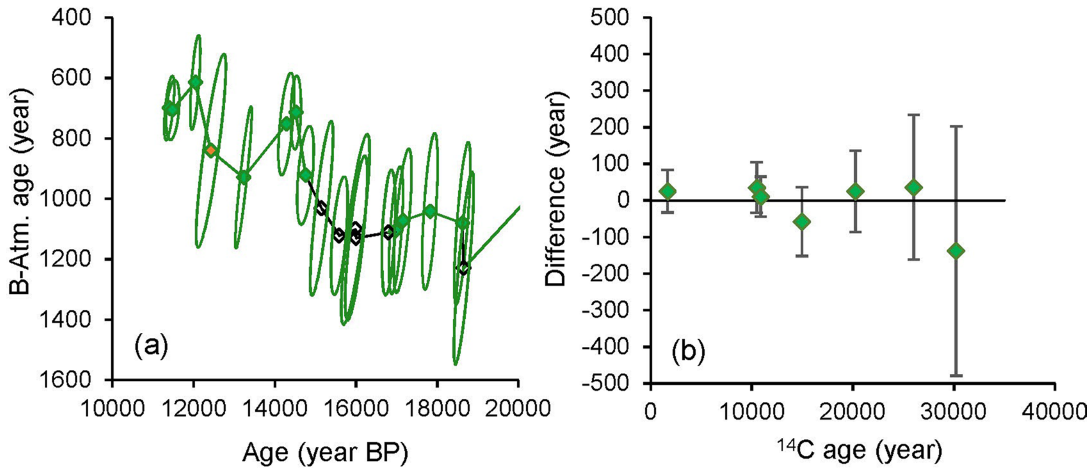

Extended Data Fig. 6 | Data comparison between published dataset and this study. (**a**) Deglacial data from low latitude intermediate Atlantic. New data of YD and HS1 presented in this study are shown by orange diamond and hollow diamond, respectively. (**b**) The difference between ^{14}C ages measured in the Bristol AMS and in the UCI AMS. Note the age differences also include the inhomogeneity of deep-sea coral samples.

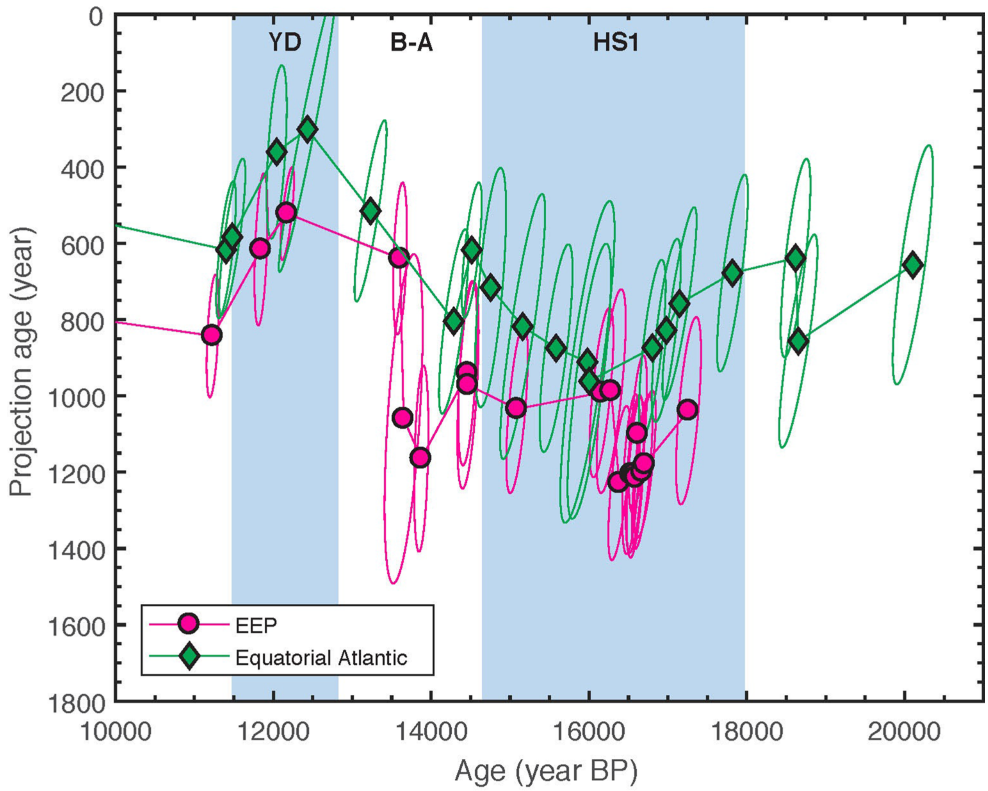

Extended Data Fig. 7 | Projection age calculated from data of the deep-sea corals in this study. Note that the coral ^{14}C data are projected to the average global surface ocean reservoir (that is, Marine13 calibration curve[39]). In this case, the projection age would be systematically lower than the B-Atm age which is compared to the atmosphere.

Region	sample name	Latitude (°N)	Longitude (°E)	Depth (m)	Age (year BP)	2 sigma	^{14}C age	2 sigma	Δ^{14}C (‰)	$\Delta\Delta^{14}$C (‰)	B-Atm (year)
Eq. Atlantic	f0001carcs001	9.216	-21.316	1080	5427	145	5425	59	-19	-94	738
Eq. Atlantic	f0001carcs027	9.216	-21.316	1080	12428	304	11329	67	97	-122	843
Eq. Atlantic	f0001carcs016	9.216	-21.316	1080	15157	230	13747	78	130	-154	1025
Eq. Atlantic	f0001carcs061	9.216	-21.316	1080	15583	167	14128	83	134	-170	1119
Eq. Atlantic	f0001carcs024	9.216	-21.316	1080	15983	284	14392	81	152	-170	1103
Eq. Atlantic	f0001carcs044	9.216	-21.316	1080	16003	220	14435	81	148	-175	1131
Eq. Atlantic	f0001carcs065	9.216	-21.316	1080	16801	138	14972	88	183	-175	1107
Eq. Atlantic	f0001carcs051	9.216	-21.316	1080	18654	198	16606	96	208	-199	1220
Galápagos	MV1007-DO9-19	0.459	-90.712	627	145	17	975	50	-99	-97	818
Galápagos	NA064-118-1-C-2A	-0.371	-90.815	419	2517	21	3343	53	-106	-101	855
Galápagos	NA064-117-01-C-2B	-0.371	-90.815	421	2942	55	3673	53	-96	-99	838
Galápagos	NA064-118-1-C-2B	-0.371	-90.815	419	3101	41	3787	53	-92	-100	841
Galápagos	MV1007-DO3-4-37	0.459	-90.712	627	11231	63	10740	69	22	-123	915
Galápagos	MV1007-DO9-2	0.787	-91.304	589	11843	68	10920	69	76	-104	741
Galápagos	MV1007-DO3-5-16	0.459	-90.712	627	12178	70	11275	71	72	-127	899
Galápagos	MV1007-DO3-4-53	0.459	-90.712	627	13604	74	12788	76	55	-137	984
Galápagos	MV1007-DO3-4-27	0.459	-90.712	627	13654	200	12943	78	41	-155	1107
Galápagos	MV1007-DO3-4-55	0.459	-90.712	627	13873	74	13079	77	51	-144	1031
Galápagos	MV1007-DO3-2-4	0.459	-90.712	627	14458	92	13379	79	87	-139	965
Galápagos	MV1007-DO3-4-60	0.459	-90.712	627	14467	114	13400	79	86	-142	985
Galápagos	MV1007-DO3-4-51	0.459	-90.712	627	15086	118	13852	80	106	-178	1202
Galápagos	MV1007-DO3-4-59	0.459	-90.712	627	16153	129	14559	85	152	-176	1139
Galápagos	MV1007-DO3-4-20	0.459	-90.712	627	16285	150	14650	86	157	-173	1114
Galápagos	MV1007-DO3-2-2	0.459	-90.712	627	16383	106	14919	88	133	-200	1306
Galápagos	MV1007-DO3-2-3	0.459	-90.712	627	16535	93	15021	88	139	-203	1313
Galápagos	MV1007-DO3-2-1	0.459	-90.712	627	16581	92	15059	88	140	-204	1322
Galápagos	MV1007-DO3-4-52	0.459	-90.712	627	16593	91	15082	89	139	-206	1333
Galápagos	MV1007-DO3-2-13	0.459	-90.712	627	16622	92	15009	89	152	-194	1245
Galápagos	MV1007-DO3-2-15	0.459	-90.712	627	16672	109	15140	89	141	-208	1342
Galápagos	MV1007-DO3-5-37	0.459	-90.712	627	16710	111	15158	90	144	-208	1344
Galápagos	MV1007-DO3-4-42	0.459	-90.712	627	17259	127	15507	91	170	-210	1329

Extended Data Table 1 | Radiocarbon data of the Galápagos deep-sea coral together with new data from the equatorial Atlantic intermediate waters. The table includes the location, depth, calendar age, ^{14}C age, Δ^{14}C, $\Delta\Delta^{14}$C, and B-Atm age of the deglacial samples reported in this study.

sample name	U-Th Age (years) after corr.	2 sigma	U-Th Age (years) before corr.	2 sigma	$\delta^{234}U_{meas}$	2 sigma	$\delta^{234}U_{initial}$	2 sigma	$[^{230}Th/^{238}U]$	2 sigma	^{238}U (ppm)	2 sigma	^{232}Th (ppt)	2 sigma
f0001carcs001	5,493	145	5631	34	146.2	1.0	148.5	1.0	0.0577	0.0003	5.12	0.01	1564	6.48
f0001carcs061	15,649	167	15737	142	144.2	1.2	150.8	1.3	0.1540	0.0013	4.49	0.02	863	5.27
f0001carcs024	16,049	284	16297	138	144.9	1.0	151.6	1.1	0.1592	0.0012	4.40	0.02	2375	12.80
f0001carcs044	16,069	220	16258	109	144.2	1.1	150.9	1.1	0.1587	0.0010	4.36	0.01	1801	8.10
f0001carcs065	16,867	138	16953	107	142.4	1.1	149.4	1.1	0.1648	0.0009	4.48	0.01	839	3.85
f0001carcs051	18,720	198	18854	146	137.8	1.1	145.3	1.1	0.1810	0.0013	4.70	0.01	1367	6.03

Extended Data Table 2 | New U-Th age data of the deep-sea corals from the equatorial Atlantic. The table includes the detailed U-series data of deep-sea corals analyzed in this study.

sample name	^{14}C age @Bristol (year)	2 sigma	^{14}C age @UCI (year)	2 sigma	Difference (year)	2 sigma
f0076carcs001	1661	52	1636*	39	25	58
f0108carcs003	10490	60	10455*	51	35	69
f0123descm001	10890	54	10880*	50	10	55
f0073carcs001	14949	74	15007*	72	-58	94
f0186carcs005	20243	108	20218*	127	25	111
f0076carcs010	26006	194	25970	240	36	197
f0183carcm001	30212	312	30350	380	-138	341

Extended Data Table 3 | Test of the coral radiocarbon age reproducibility between AMS in UCI and Bristol. The table includes ^{14}C data measured by accelerator mass spectrometer in the University of Bristol as well as the University of California Irvine. Data published in Chen et al.[13].